AIAA SciTech Forum
8-12 January 2024, Orlando, FL
AIAA SCITECH 2024 Forum

10.2514/6.2024-1636

VLE-Based High Pressure Stationary Droplet Evaporation at Spray Detonation Conditions

Navneeth Srinivasan *[1], Suryanarayan Ramachandran †[1], Hongyuan Zhang ‡[1], Abeetath Ghosh §[2], Sai Sandeep Dammati ¶[2], Alexei Poludnenko ‖[2], and Suo Yang **[1]
[1]*Department of Mechanical Engineering, University of Minnesota – Twin Cities, Minneapolis, MN 55455, USA*
[2]*Department of Mechanical Engineering, University of Connecticut, Storrs, CT 06269, USA*

This paper numerically investigates the evaporation characteristics of a single n-dodecane fuel droplet in high-pressure nitrogen environment relevant to rotating detonation engines. A validated computational fluid dynamics solver coupled with real-fluid thermophysical models is utilized. The effects of pressure, droplet temperature, and ambient gas temperature on the evaporation rate are analyzed by tracking the droplet diameter evolution. Two interface tracking techniques, namely a mean density-based method and a novel vapor-liquid equilibrium-based method, are implemented and compared. The results show appreciable deviations from the classical D^2-law for droplet evaporation. Increasing the ambient temperature and droplet temperature (toward critical point) substantially accelerate the evaporation process. Meanwhile, higher pressures decrease the evaporation rate owing to slower species/thermal diffusions. At certain conditions, discernible differences are observed between the two interface tracking methods indicating deficiencies in the simple mean density approach. The paper demonstrates an effective computational framework for transcritical droplet evaporation simulations. And the generated high-pressure droplet evaporation datasets can inform sub-model development for spray combustion modeling.

Downloaded by Suo Yang on January 4, 2024 | http://arc.aiaa.org | DOI: 10.2514/6.2024-1636

I. Introduction

Evaporation of spherical droplets in gaseous environments has wide applications in engineering such as spray combustion, cooling, drying etc. Droplet evaporation is a complex two-phase multi-physics phenomena, which includes liquid heating, fluid convection, thermodynamic variations etc. [1]. Droplet evaporation was classically modeled by the D^2 law, which predicts that the square of the droplet diameter decreases linearly with time. Since then, many advances in droplet evaporation have been reported including the effect of variable thermophysical properties, non-unity Lewis number, transient liquid heating and non-equilibrium evaporation assumption [2].

Among the multiple options available for evaporation models, the most commonly used model was developed by Abramzon and Sirignano [3]. This model was developed about 30 years ago and is still widely used in many liquid droplet simulations primarily because of its efficient implementation in CFD codes. This model is based on the one dimensional “stagnant film theory”, incorporating the Stefan flow effect on the thicknesses of the thermal and diffusional films. However, the applicability of the model to supercritical environments is still not clear. Recent work by Dammati et al. [4] showcased the thermophysical conditions experienced by fuel droplets in rotating detonation engine (RDE) environments.

Figures 1, 2 show the distribution of the thermophysical conditions of $C_{12}H_{26}$ droplets experienced in a planar detonation front environment. N-Dodecane ($C_{12}H_{26}$), used here as the fuel, has a critical temperature of 658 K and critical pressure of 18 bar. The figure shows that the most commonly occurring state of droplets is close to 20 bar and 620 K. This puts droplets close to their critical point showcasing the importance of considering transcritical phase change while estimating the droplet evaporation rate. Since this case uses a single component fuel, the critical point is very close to its injection conditions, but most fuels used commonly are multi-component and have higher mixture critical points compared to their individual components as shown by Zhang et al. [5].

---

[*] Ph.D. Candidate, srini237@umn.edu, Student Member AIAA.
[†] Ph.D. Student, ramac106@umn.edu, Student Member AIAA.
[‡] Ph.D. Candidate, zhan6305@umn.edu, Student Member AIAA.
[§] Ph.D. Student, Student Member AIAA.
[¶] Postdoc, Member AIAA.
[‖] Associate Professor, Member AIAA.
[**] Richard & Barbara Nelson Assistant Professor, suo-yang@umn.edu (Corresponding Author), Senior Member AIAA.

Copyright © 2024 by Navneeth Srinivasan, Suryanarayan Ramachandran, Hongyuan Zhang, Abeetath Ghosh, Sai Sandeep Dammati, Alexei Poludnenko and Suo Yang .
Published by the American Institute of Aeronautics and Astronautics, Inc., with permission.

Downloaded by Suo Yang on January 4, 2024 | http://arc.aiaa.org | DOI: 10.2514/6.2024-1636

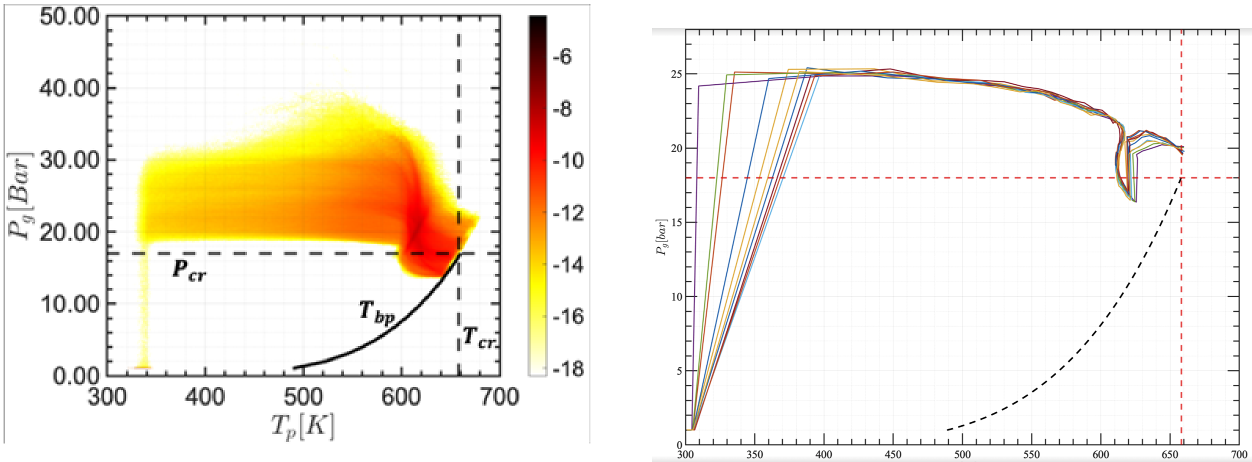

((a)) Joint PDF of the gas pressure and temperature experienced by the droplets in a 2D detonation front

((b)) Samples of droplet trajectories in PT space

Fig. 1 Droplet number density distribution in thermodynamic space (figures from Dammati et al. [4]).

With ever increasing demand for high performance combustors, increasing the chamber pressure is one often sought after option [6, 7]. This leads to the working conditions to overlap with the supercritical regime of the reactants. Due to the high-pressure environment in engine combustors, the injected multi-component liquid propellants and fuel-air mixtures often go through thermodynamically transcritical processes during the spray breakup, evaporation, mixing and combustion processes. Efficient spray breakup and evaporation of liquid fuels are the primary targets of engine combustor design and control to ensure sufficiently small "effective" evaporation time. The existing liquid fuel injectors and multi-component liquid fuels developed for low pressures are not optimal at high pressures, and hence require redesign and optimization.

To understand the subcritical and supercritical mixing process, a simulation tool is needed. Since supercritical region is far from the ideal gas region, real-gas effect needs to be considered to capture correct behavior. In addition, transcritical and supercritical fluid behavior can be peculiar because of the large variation of thermophysical properties, such as density and specific heat near the critical point. As a result, the Computational Fluid Dynamics (CFD) modeling of supercritical flows is very challenging. Since small changes in temperature and pressure can have large effects on the structure of a fluid near the critical point, local properties are very important. Furthermore, a supercritical fluid lacks surface tension, which means modeling of transcritical flow requires one to capture the surface tension change when the fluid goes across phase boundary. This makes simulation of transcritical flow more challenging than supercritical flow.

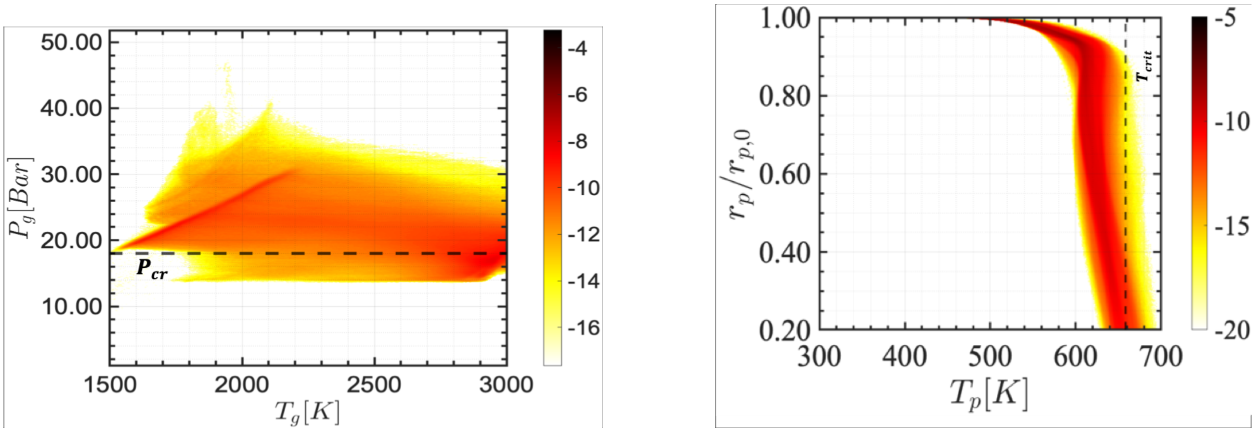

((a)) Joint PDF of the ambient gas pressure and droplet temperature in a 2D detonation front

((b)) Joint PDF of the normalized droplet radius and droplet temperature in a 2D detonation front

Fig. 2 Droplet properties in a 2D detonation front (figures from Dammati et al. [4]).

Downloaded by Suo Yang on January 4, 2024 | http://arc.aiaa.org | DOI: 10.2514/6.2024-1636

The studies of transcritical and supercritical injection and mixing have attracted much interest in the past 30 years. However, most of them were mainly concentrated on the single-component system, whose critical point is a constant value. As long as the fluid exceeds its critical point, it goes into the supercritical state, and the classical "dense-fluid" approach is used with the assumption of a single-phase [8]. Since the real mixture critical pressure could be significantly higher than the critical pressure of each component [9], the accurate mixture critical point needs to be obtained.

Recently, several studies focus on multi-component transcritical flow simulation, capturing the phase separation at high pressure. Most works use the vapor-liquid equilibrium (VLE) theory to capture phase separation. Yao et al. [10] developed a fluids solver based on VLE to investigate the impact of diffusion models of a laminar counter-flow flame at trans- and supercritical conditions. In Ray et al.'s work [11], VLE theory is used to understand fuel droplet evaporation at high pressures. A similar framework is also used in Tudisco and Menon's [12] works to understand the effect of Lewis number .

A complete droplet evaporation rule for transcritical fluid operating regions is still an open research question. This work focuses on simulating a stationary single droplet of fuel in an inert medium to obtain equivalent high-pressure evaporation laws using a novel VLE-based interface tracking technique. The numerical methods adopted to sufficiently account for high-pressure transcritical effects are outlined and the novel VLE-based interface tracking algorithm is explained in Sec. II. The resulting droplet evaporation laws at the detonation-relevant thermodynamic space is presented in Sec. III.

II. Numerical Methods

A. Models of thermodynamic and transport properties

Here, we use VLE solvers to capture the phase change and determine the critical point of a multi-component mixture in a transcritical flow as described above. VLE describes the phase equilibrium between liquid and vapor phases and solving the set of VLE equations gives the phase fraction and compositions in the two phases. If the gas (vapor) phase mole fraction is equal to 0 or 1, then the system is in a purely liquid or gaseous phase respectively. If the system falls into the two-phase region, gas phase mole fraction will be between 0 and 1, and an equilibrium between vapor and liquid will be observed. If at certain conditions, thermodynamic properties become identical between liquid and gas, it indicates the occurrence of the transcritical transition from a subcritical state to a supercritical state, which could be either a liquid-like or gas-like state.

The fluid solver that is implemented is coupled with the isobaric and isenthalpic (PHn) flash solver [13]. PHn flash and almost all other VLE solvers, are developed based on TPn flash. Specifically, PHn flash solves the VLE equation set at given enthalpy (H) rather than temperature. TPn flash is the most basic VLE solver, which solves the set of VLE equations at the given temperature (T), pressure (P), and mole fraction of each component (n) in the system.

Isothermal and isobaric (TPn) flash: VLE is governed by fugacity equality Eq. (1) and Rachford-Rice equation [14] Eq. (2), which is an additional constraint to the equilibrium solver as used in Saha and Carroll [15] and obtained from the conservation of each component:

$$f_{i,l} \big/ f_{i,g} = 1 \tag{1}$$

$$\sum_{i=1}^{N} \left\{ z_i \left(1 - K_i\right) \Big/ \left[1 + \left(K_i - 1\right) \psi_g\right] \right\} = 0 \tag{2}$$

$$K_i = y_i / x_i \tag{3}$$

$$\sum_{i=1}^{N} x_i = \sum_{i=1}^{N} y_i = 1 \tag{4}$$

where $f_{i,p}$ is the fugacity of component i in phase p ($p = l$: liquid; $p = g$: gas), x_i is the mole fraction of component i in liquid phase, y_i is the mole fraction of component i in gas phase, z_i is the mole fraction of component i in the feed (i.e., the whole mixture including both gas phase and liquid phase), ψ_g is the gas mole fraction, K_i is the equilibrium constant of component i.

The real fluid properties are described using the Peng-Robinson equation of state (PR-EOS) [16] as:

$$P = \frac{RT}{V - b} - \frac{a}{V\left(V + b\right) + b\left(V - b\right)} \tag{5}$$

Downloaded by Suo Yang on January 4, 2024 | http://arc.aiaa.org | DOI: 10.2514/6.2024-1636

where P, R, T and V are pressure, gas constant, temperature, and specific volume, respectively. For a single-component fluid, the PR-EOS parameters are given by

$$a = 0.45724\frac{R^2T_c^2}{p_c}\hat{a}, \qquad b = 0.07780\frac{RT_c}{p_c}, \tag{6}$$

$$\hat{a} = \left(1+\kappa\left(1-(T_r)^{1/2}\right)\right)^2, \qquad \kappa = 0.37464 + 1.54226\omega - 0.26992\omega^2 \tag{7}$$

where subscript "c" means critical value, subscript "r" means the reduced value (e.g., $T_r = T/T_c$), ω is acentric factor.

The liquid phase and the gas phase are described by the two multi-component PR-EOS, respectively. The specific volume of each phase, V_p, is solved from PR-EOS. The compressibility factor of each phase ($Z = PV/RT$) can also be obtained from this.

The fugacity formula of PR-EOS is shown below [17]:

$$f_i = P\chi_i \exp\left[\frac{B_i}{B_{mix}}(Z-1) - ln(Z - B_{mix}) - \frac{A_{mix}}{2\sqrt{2}B_{mix}}\left(\frac{2\sum_j x_j A_j}{A_{mix}} - \frac{B_i}{B_{mix}}\right) ln\left(\frac{Z+(1+\sqrt{2})B_{mix}}{Z+(1-\sqrt{2})B_{mix}}\right)\right] \tag{8}$$

where χ_i is the mole fraction of component i (for liquid, $\chi_i = x_i$; for gas phase, $\chi_i = y_i$),

$$A_i = \frac{a_i p}{R^2T^2}, \tag{9}$$

$$B_i = \frac{b_i p}{RT}, \tag{10}$$

$$A_{mix} = \sum_i \sum_j x_i x_j (1 - b_{ij})\sqrt{A_i A_j}, \tag{11}$$

$$B_{mix} = \sum_i x_i B_i \tag{12}$$

The equation set Eq. (1-12) is solved using Newton iteration method. The flow chart of the TPn flash is shown in Fig. 3. The initial guess is obtained using Wilson Equation [18]:

$$K_i = e^{5.373(1+\omega_i)(1-1/T_{r,i})}/P_{r,i} \tag{13}$$

where ω_i is the acentric factor of component i; $T_{r,i}$ and $P_{r,i}$ are the reduced temperature and reduced pressure of component i, respectively.

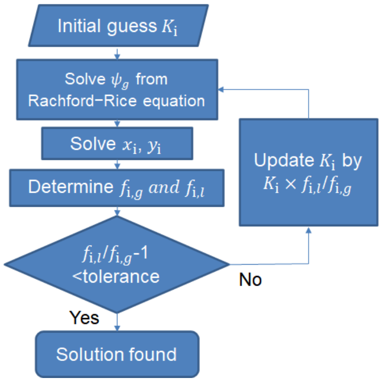

Fig. 3 Flow chart of the TPn flash solver.

PV flash and UV flash: The PV flash and UV flash solvers are developed based on the TP flash. Both of them use iteration methods. Specifically, initial guesses (T for PV flash; T and P for UV flash) are obtained from the previous time step, and a TP flash problem is solved in each iteration. After several iterations, when the error is smaller than tolerance, the solver returns a solution.

In PV flash, since pressure (P) is already given as an input, only temperature (T) needs to be guessed and updated during the iteration. A secant method is used to avoid the expensive derivative computation in the Newton-Raphson

Downloaded by Suo Yang on January 4, 2024 | http://arc.aiaa.org | DOI: 10.2514/6.2024-1636

method. In UV flash, two variables (both T and P) need to be guessed and updated simultaneously during the iteration, and hence the secant method cannot be applied. The Newton-Raphson method is used to solve the UV flash problems. The required Jacobian matrix is obtained using the analytical framework of Tudisco and Menon [19].

Transport properties: The dense fluid formula [20] is used to evaluate the dynamic viscosity and thermal conductivity under transcritical conditions. This method gives accurate estimations of viscosity and thermal conductivity of polar, non-polar and associating pure fluids and mixtures. Its dynamic viscosity and thermal conductivity have a similar formula:

$$\lambda = \lambda_0 \lambda^* + \lambda_p \tag{14}$$

where λ represents dynamic viscosity or thermal conductivity. λ_0 is the gas property at low pressures. λ^* and λ_p are high-pressure corrections. At high pressures, λ_p is the major contributing term comparing to $\lambda_0\lambda^*$. On the other hand, at low pressures, λ^* is approaching unity, and the λ_p term is negligible such that Eq. 14 reduces to λ_0. Hence, the transition between subcritical and supercritical states is smoothly described by the model. For mass diffusivity, we used mixture-averaged mass diffusion model. The mass diffusion coefficient of species i, D_i, which is defined by [21] is,

$$D_i = \frac{1 - Y_i}{\sum_{j \neq i}^{N} X_j / D_{j,i}} \tag{15}$$

where Y_i and X_i are the mass and mole fractions of i-th species, respectively; $D_{i,j}$ is the binary diffusion coefficient, which is evaluated by Fuller's model [22] with Takahashi's correction [23].

B. CFD Flow Solver Formulation

The equation of mass conservation, momentum (neglecting body force), energy, together with species transport can be written as

$$\frac{\partial \rho}{\partial t} + \nabla \cdot (\rho u) = 0; \tag{16}$$

$$\frac{\partial \rho u}{\partial t} + \nabla \cdot (\rho u \otimes u) = -\nabla p + \nabla \cdot \tau; \tag{17}$$

$$\frac{\partial \rho E}{\partial t} + \nabla \cdot (\rho E u) = -\nabla \cdot (u p) + \nabla \cdot (u \cdot \tau) + \nabla \cdot q; \tag{18}$$

$$\frac{\partial \rho Y_s}{\partial t} + \nabla \cdot (\rho Y_s u) = -\nabla \cdot j_s + \rho \dot{\omega}_s, \qquad s = 1, ..., n_s; \tag{19}$$

where ρ is the mixture density, p is the pressure, $\boldsymbol{u}$ is the velocity, τ is the viscous stress tensor, $\boldsymbol{q}$ is the heat flux, $E = e + \frac{1}{2} u \cdot u$ is the total energy. In Eq. (19), Y_s, j_s and $\dot{\omega}_s$ are the mass fraction, diffusion mass flux and production rate of species s, while n_s is the total number of species. However, based on our preliminary tests that solved the full governing system, we note that there is no appreciable change in the pressure of the system. Furthermore, since Stefan flow effects are neglected, vaporization-induced flow velocities do not arise in our system and hence all components of the velocity were found to be negligible. Consequently, we solve only for the energy and species conservation (i.e. Eqs. 18 and 19). The pressure of the system is imposed to be constant using which the density is now updated using the PR-EOS.

C. Solution methodology, Domain & Configuration

The governing equations are solved using a well-validated open-source OpenFOAM-based reacting flow solver –*realFluidReactingFoam* [24] that accounts for high-pressure transport and non-ideal, real-fluid equations of state. Since we deal with the evaporation of a stationary droplet, we use the PIMPLE algorithm to advance the governing equation system in a low-Mach setting to allow for larger time-steps during numerical integration. We employ a three-dimensional cubic domain with a side of $l = 600\mu$m spanning 128^3 cells (fetching a resolution of $\Delta x = \Delta y = \Delta z = 0.47\mu$m ensuring we are well above the continuum limit which is in the $O(nm)$) shown in Fig. 4. The evaporation of a stationary spherical n-dodecane droplet of initial diameter $D_0 = 30\mu$m placed at the center of the domain is studied at a range of thermodynamic conditions. The droplet diameter is chosen based on the typical droplet size encountered in RDEs [25] and diesel-engines [26]. The thermodynamic conditions are chosen based on the most probable states a droplet experiences when it encounters a typical 2D detonation. These states are chosen where the Probability Density Function

Downloaded by Suo Yang on January 4, 2024 | http://arc.aiaa.org | DOI: 10.2514/6.2024-1636

(PDF) of the droplet number density in Fig. 1 is most populated (i.e. attains a maximum). Following this reasoning, it can be easily seen that the most probable pressures experienced by the droplet are between 15 − 30bar with the droplet temperatures falling in the range of $T_d = 500 - 680$K (see Fig.1(a)). Note that the critical pressure and temperature of n-dodecane is $P_c = 18$bar, $T_c = 660$K. Consequently, we study two droplet temperatures $T_d = 550\&650$K with the former representing a sub-critical temperature and the latter representing a near-critical temperature thereby allowing for trans-critical phase-change in both cases. Four pressures namely, $p = 15, 20, 25, \&30$ bar and ambient temperatures, $T_a = 800, 1000, \&1500$K are studied to fully span the most probable pressure space (see Fig. 1(a)). The ambient temperatures are chosen based on Fig. 2(a) where the lower limit of the ambient temperature is $T_a = 1500$K. At higher temperatures we note that the the probability of auto-ignition of the droplet [25] is higher due to which evaporation timescales are expected to be smaller than reaction timescales. Consequently we study two lower temperatures $T_a = 800\&1000$K. A zero-gradient Neumann boundary condition on all the variables is imposed at all the boundaries of the cubical domain.

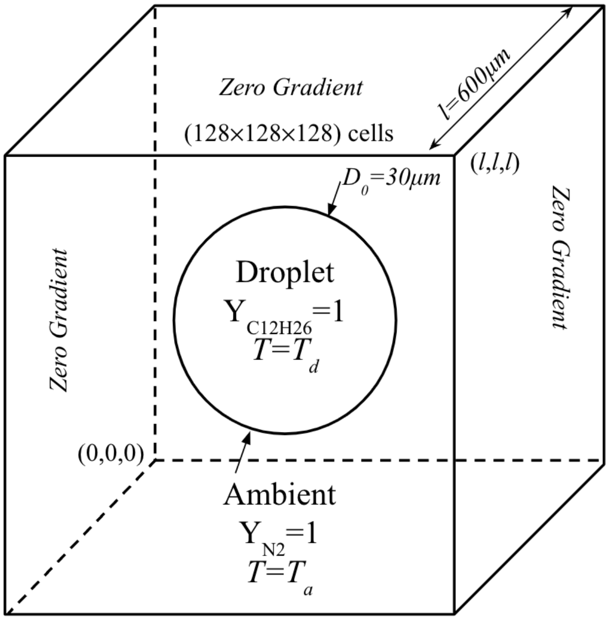

Fig. 4 The three-dimensional domain used to study the evaporation of a single n-dodecane droplet in nitrogen.

Two interface tracking techniques are investigated and compared against each other. The first method used follows the work of Ly *et al.* [27] and Xiao *et al.*[28] where the mean density of the droplet and the ambient nitrogen is tracked as time progresses. Such a method is the most commonly used technique and is suited to match experiments where schlieren images are the only mode of inference on the droplet interface. However, we question the applicability of this method fundamentally in light of the availability of better data via computations due to the fact that mean density can only estimate the true location of the two-phase zone during the evaporation of the droplet. Strictly speaking, one must track the location where the mole-fraction of the net liquid and the vapour phases are equal to each other i.e. the vapour fraction $\phi_v = 0.5$ as such a location is most representative of the two-phase zone. Whether this holds for the density-based indicator is questioned and analyzed in this study by examining the second indicator $\beta = \phi_v(1 - \phi_v)$ based on the local vapor fraction ϕ_v. To the best of the authors' knowledge, this is the first of such works to investigate this aspect of droplet evaporation. Such an interface tracking method requires expensive VLE computations at every grid cell. Consequently, very expensive 0-D VLE flash solvers need to be coupled with the CFD solver (see Zhang and Yang [29] and Srinivasan *et al.* [30]) employed which presents itself as a challenge. Furthermore, acceleration techniques such as ISAT [29, 31] also need to be implemented to reduce the time needed for post-processing every timestep. To alleviate these challenges, we adopt the Artificial Neural Network (ANN)-based approach outlined in Srinivasan *et al.* [32] which is a very user-friendly, plug-and-play approach to convert any CFD solver into a multi-phase VLE based solver. This is demonstrated in this work by coupling a pre-trained ANN that tabulates the vapour-fraction ϕ_v for the chosen thermodynamic space to the OpenFOAM-based solver, *realFluidReactingFoam* via the ONNX runtime environment [33, 34] to enable fast inference of trained ANN models. The ANN is the called locally at every grid-cell

Downloaded by Suo Yang on January 4, 2024 | http://arc.aiaa.org | DOI: 10.2514/6.2024-1636

and the local value of the interface tracker $\beta = \phi_v(1 - \phi_v)$ is computed. The droplet interface is defined as those locations where $\beta = 0.25$ (i.e. where $\phi_v = 0.5$) and these points are then tracked and stored similar to the mean density.

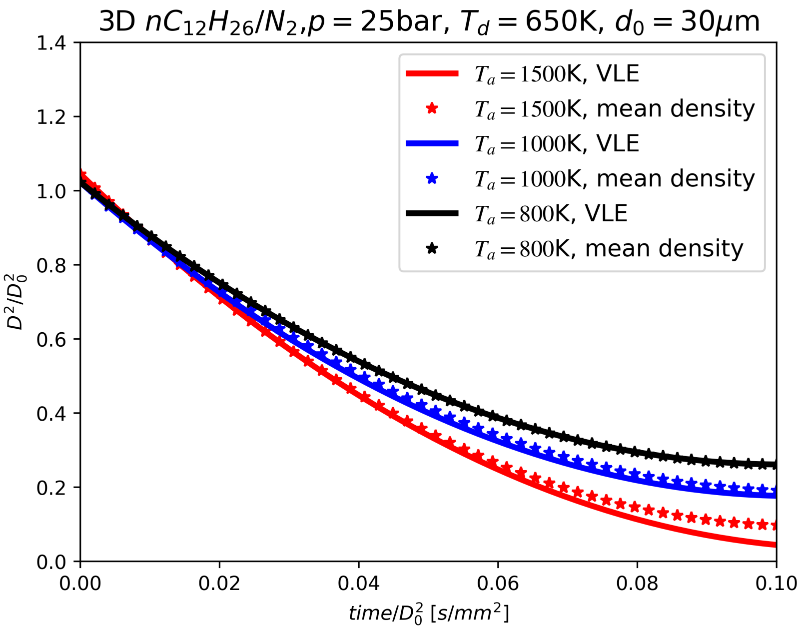

((a)) Dependence on ambient temperature T_a

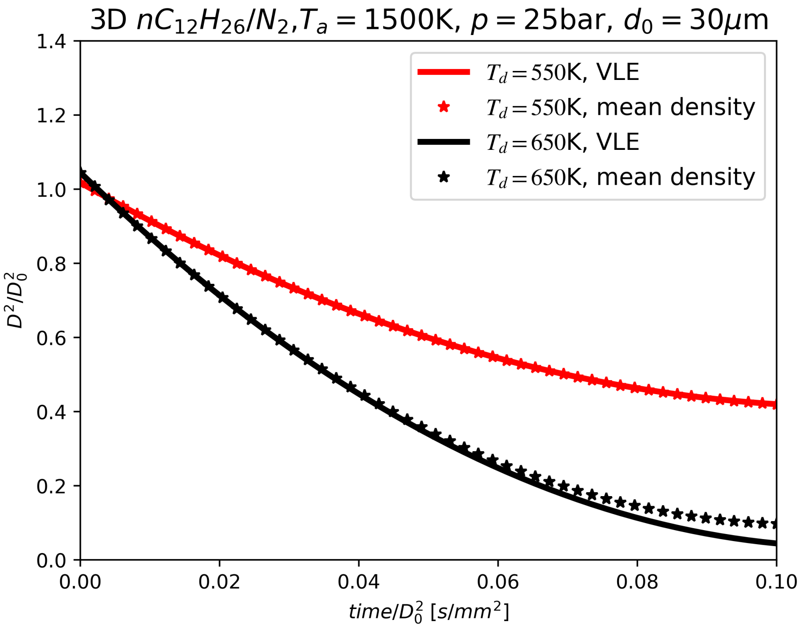

((b)) Dependence on the droplet temperature T_d

Fig. 5 Dependence on the droplet (T_d) and ambient temperature (T_a) on the evaporation rate of a stationary n-dodecane droplet in N_2.

Downloaded by Suo Yang on January 4, 2024 | http://arc.aiaa.org | DOI: 10.2514/6.2024-1636

III. Results

Temperature effects namely the dependence of the droplet temperature (T_d) and the ambient temperature (T_a) are first studied for the two indicators in Sec. III.A. Subsequently, the effect of pressure is studied in Sec. III.B.

A. Temperature dependence

Following the typical d^2-law, we examine the evolution of the square of the non-dimensionalized droplet diameter (D^2/D_0^2) in for the both the interface indicators for various ambient and droplet temperatures considered in Fig. 5.

The most probable pressure $P = 25$ bar and droplet temperature $T_d = 650$K is used while the ambient temperature is varied in Fig. 5(a). Several interesting observations follow from this plot. Firstly, if indeed the D^2-law holds, the obtained plots should have had constant evaporation rates (i.e. straight lines) which is clearly not the case as visible from Fig. 5(a). Due to slower diffusion at higher (and near-critical) pressures, the evaporation seems to happen slower as time proceeds (evident from the gradual tapering of the curves in contrast to a steep decrease). Secondly, we note that at higher ambient temperatures the droplet evaporates faster. This observation is consistent with the fact that at higher ambient temperatures, the temperature gradient between the droplet and the ambient is higher due to which the heat-conduction rate ($\propto \kappa \nabla T$) is higher. Consequently the droplet heats up faster and undergoes faster evaporation. Finally, we note the performance of the two indicators implemented. At $T_a = 800$K, the two indicators namely, mean-density and VLE-based, seem to agree with each other to a large extent. However small discrepancies (about $5-6\%$ mean-absolute error) are noted at a slightly higher temperature of $T_a = 1000$K. Towards the end of the droplet lifetime, even larger discrepancies are observed at the higher ambient temperature of $T_a = 1500$K. We explain this based on the fact that at higher temperatures the two-phase zone is expected to be thicker due to larger temperature gradients in the system. Consequently, VLE-based indicators are able to account for this effect accurately.

The effect of the droplet temperature is studied in Fig. 5(b) while holding the ambient temperature at $T_a = 1500$K. We note that a similar trend is observed i.e. at the lower droplet temperature of $T_d = 550$K the evaporation rate is observed to be slower due to lower heat-transfer rates while the vice-versa holds at the higher droplet temperature of $T_d = 650$K. Nonetheless, it is interesting to note that for a 100K increase in the droplet temperature, the evaporation rate seems to have increased more rapidly than a 700K increase in the ambient temperature. Note that the $(D/D_0)^2$ at the end of $t/{D_0}^2 = 0.1$ seems to have dropped only by a factor of 2 for a 700K rise in T_a (from $T_a = 800$K to $T_a = 1500$K). In contrast for a 100K rise (from $T_d = 550$ to 650K) however, there is a drop from $D/D_0^2 = 0.4$ to 0.1 (i.e. four-fold), illustrating that pushing the droplet temperature near the critical point seems to have a stronger effect and (i.e. transcritical phase change) proceeds differently compared to the effect of ambient temperature.

B. Pressure Dependence

The near-critical droplet temperature $T_d = 650$K and the highest ambient temperature $T_a = 1500$K is used study the effect of pressure. The density-based indicator is used to infer on the trends as qualitatively the two indicators seem to perform well based on the temperature effect. The resulting evolution of the non-dimensionalized droplet diameter is plotted in Fig. 6 for the four pressures considered. Note that $p = 15$ bar is a sub-critical pressure while the other pressures are super-critical following the fact the critical pressure $p_c = 18$ bar. A clearly visible trend from the plot is the fact that lower pressures promote faster evaporation of the droplet due to faster diffusion rates. Both thermal conductivity and species binary diffusion coefficients have an an inverse dependence on pressure [24] due to which higher pressures result in slower evaporation rates indicating that the model/solver follows the expected behavior.

IV. Conclusions and Future Work

The evaporation of a single $n-$dodecane droplet in N_2 environment was investigated at detonation-relevant conditions. The most-probable thermodynamic conditions experienced by a droplet when it encounters a detonation wave are dispersed around the critical point necessitating the use of real-fluid vapour-liquid equilibrium-based evaporation laws. Following this observation, four pressures $p = 15, 20, 25, \&30$ bar, two droplet temperatures, $T_a = 550, 650$K and three ambient temperatures $T_a = 800, 1000, \&1500$K are considered and the trends in the droplet evaporation rate are gathered using an open-source, OpenFOAM-based high-pressure real-fluid CFD solver *realFluidReactingFoam* [24]. To track the droplet radius at each time-instant, two interface tracking techniques namely a mean-density indicator and a Vapour Liquid Equilibrium (VLE)-based indicator are implemented and tested. To enable fast VLE computations, the use of a novel, user-friendly, plug-and-play Artificial Neural Network (ANN) model is demonstrated within the OpenFOAM environment. The following are the key conclusions from the study:

Downloaded by Suo Yang on January 4, 2024 | http://arc.aiaa.org | DOI: 10.2514/6.2024-1636

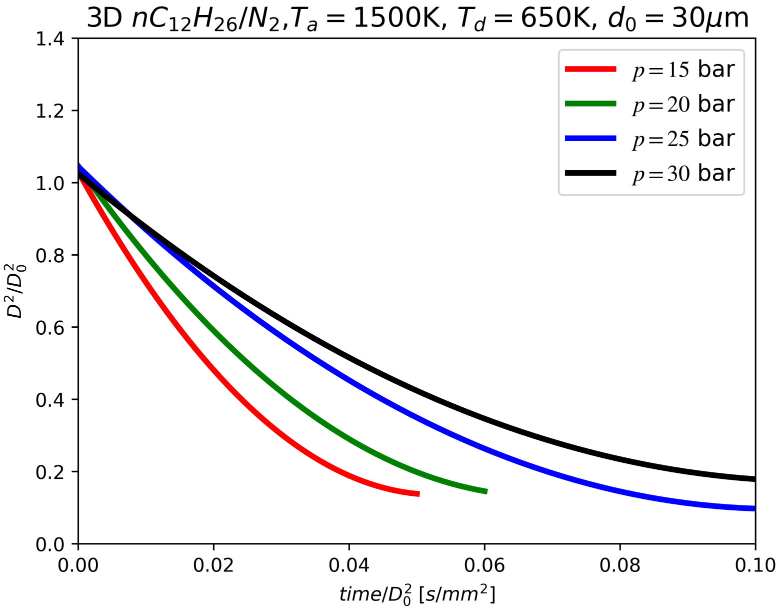

Fig. 6 Depedence on the system pressure (P) on the evaporation rate of a stationary n-dodecane droplet in N_2.

1) A deviation from the classical D^2-law behavior with the use of real-fluid equation of state and corrected high-pressure transport is noticed in the droplet-evaporation rate.
2) A rise in ambient temperature promotes faster evaporation due to higher heat-transfer rates enabled by larger temperature gradients in the system.
3) As the temperature of the droplet is pushed closer to the critical point (keeping all other parameters the same), the evaporation rate is found to increase. This effect is found to be more pronounced than the effect of the increasing the ambient temperature.
4) As the pressure of the system is increased, slower diffusion (of both species and heat) leads to a reduction in the evaporation rate.
5) The mean-density and VLE-based indicators agree with each other to a large extent. Small discrepancies $(5-6\%)$ are however noticed between two indicators. Deviations are found to be higher at higher ambient temperatures.

Future work will focus on validation with experiments at high-pressure available in current literature and the performance of the indicators pitted against experimental data. A reduced-order model for enabling fast implementation droplet evaporation models into lagrangian-based CFD codes will also be explored with other existing open-source CFD software.

Acknowledgments

S. Yang gratefully acknowledges the support from the Office of Naval Research (ONR) grant under Award No. N00014-22-1-2287 under the supervision of project monitor Dr. Steven Martens, and the National Science Foundation (NSF) grant under Award No. CBET 2023932. The authors gratefully acknowledge the computing resources provided by the Minnesota Supercomputing Institute (MSI).

References

[1] Tonini, S., and Cossali, G. E., "A novel vaporisation model for a single-component drop in high temperature air streams," *International Journal of Thermal Sciences*, Vol. 75, 2014, pp. 194–203.

[2] Aggarwal, S., and Peng, F., "A review of droplet dynamics and vaporization modeling for engineering calculations," 1995.

[3] Abramzon, B., and Sirignano, W. A., "Droplet vaporization model for spray combustion calculations," *International journal of heat and mass transfer*, Vol. 32, No. 9, 1989, pp. 1605–1618.

Downloaded by Suo Yang on January 4, 2024 | http://arc.aiaa.org | DOI: 10.2514/6.2024-1636

[4] Dammati, S. S., Kozak, Y., and Poludnenko, A., "Droplet Dynamics Characterization in Spray Detonations of Hydrocarbon Fuels," *Bulletin of the American Physical Society*, 2022.

[5] Zhang, H., Yi, P., and Yang, S., "Multicomponent Effects on the Supercritical CO2 Systems: Mixture Critical Point and Phase Separation," *Flow, Turbulence and Combustion*, Vol. 109, No. 2, 2022, pp. 515–543.

[6] Jofre, L., and Urzay, J., "Transcritical diffuse-interface hydrodynamics of propellants in high-pressure combustors of chemical propulsion systems," *Progress in Energy and Combustion Science*, Vol. 82, 2021, p. 100877.

[7] Ramachandran, S., Srinivasan, N., Taneja, T. S., Zhang, H., and Yang, S., "Numerical study of turbulent non-premixed cool flames at high and supercritical pressures: Real gas effects and dual peak structure," *Combustion and Flame*, Vol. 249, 2023, p. 112626.

[8] Yang, V., "Modeling of supercritical vaporization, mixing, and combustion processes in liquid-fueled propulsion systems," *Proceedings of the Combustion Institute*, Vol. 28, No. 1, 2000, pp. 925–942.

[9] Van Konynenburg, P., and Scott, R., "Critical lines and phase equilibria in binary van der Waals mixtures," *Philosophical Transactions of the Royal Society of London. Series A, Mathematical and Physical Sciences*, Vol. 298, No. 1442, 1980, pp. 495–540.

[10] Yao, M. X., Hickey, J.-P., Ma, P. C., and Ihme, M., "Molecular diffusion and phase stability in high-pressure combustion," *Combustion and Flame*, Vol. 210, 2019, pp. 302–314.

[11] Ray, S., Raghavan, V., and Gogos, G., "Two-phase transient simulations of evaporation characteristics of two-component liquid fuel droplets at high pressures," *International Journal of Multiphase Flow*, Vol. 111, 2019, pp. 294–309.

[12] Tudisco, P., and Menon, S., "A vapor–liquid equilibrium induced Lewis number effect in real-gas shear layers: A theoretical study," *Physics of Fluids*, Vol. 32, No. 11, 2020, p. 112111.

[13] Michelsen, M. L., "Multiphase isenthalpic and isentropic flash algorithms," *Fluid phase equilibria*, Vol. 33, No. 1-2, 1987, pp. 13–27.

[14] Rachford Jr, H., Rice, J., et al., "Procedure for use of electronic digital computers in calculating flash vaporization hydrocarbon equilibrium," *Journal of Petroleum Technology*, Vol. 4, No. 10, 1952, pp. 19–3.

[15] Saha, S., and Carroll, J. J., "The isoenergetic-isochoric flash," *Fluid phase equilibria*, Vol. 138, No. 1-2, 1997, pp. 23–41.

[16] Peng, D.-Y., and Robinson, D. B., "A new two-constant equation of state," *Industrial & Engineering Chemistry Fundamentals*, Vol. 15, No. 1, 1976, pp. 59–64.

[17] Yi, P., Yang, S., Habchi, C., and Lugo, R., "A multicomponent real-fluid fully compressible four-equation model for two-phase flow with phase change," *Physics of Fluids*, Vol. 31, No. 2, 2019, p. 026102.

[18] Wilson, G. M., "Vapor-liquid equilibrium. XI. A new expression for the excess free energy of mixing," *Journal of the American Chemical Society*, Vol. 86, No. 2, 1964, pp. 127–130.

[19] Tudisco, P., and Menon, S., "Analytical framework for real-gas mixtures with phase-equilibrium thermodynamics," *The Journal of Supercritical Fluids*, Vol. 164, 2020, p. 104929.

[20] Chung, T. H., Ajlan, M., Lee, L. L., and Starling, K. E., "Generalized multiparameter correlation for nonpolar and polar fluid transport properties," *Industrial & engineering chemistry research*, Vol. 27, No. 4, 1988, pp. 671–679.

[21] Kee, R. J., Rupley, F. M., Meeks, E., and Miller, J. A., "CHEMKIN-III: A FORTRAN chemical kinetics package for the analysis of gas-phase chemical and plasma kinetics," Tech. rep., Sandia National Lab.(SNL-CA), Livermore, CA (United States), 1996.

[22] Fuller, E. N., Schettler, P. D., and Giddings, J. C., "New method for prediction of binary gas-phase diffusion coefficients," *Industrial & Engineering Chemistry*, Vol. 58, No. 5, 1966, pp. 18–27.

[23] Takahashi, S., "Preparation of a generalized chart for the diffusion coefficients of gases at high pressures," *Journal of Chemical Engineering of Japan*, Vol. 7, No. 6, 1975, pp. 417–420.

[24] Nguyen, D. N., Jung, K. S., Shim, J. W., and Yoo, C. S., "Real-fluid thermophysicalModels: An OpenFOAM-based library for reacting flow simulations at high pressure," *Computer Physics Communications*, Vol. 273, 2022, p. 108264.

[25] Prakash, S., Bielawski, R., Raman, V., Ahmed, K., and Bennewitz, J., “Three-dimensional Numerical Simulations of a Liquid RP-2/O2 based Rotating Detonation Engine,” *Combustion and Flame*, Vol. 259, 2024, p. 113097.

[26] Li, G., Cao, J., Li, M., Quan, Y., and Chen, Z., “Experimental study on the size distribution characteristics of spray droplets of DME/diesel blended fuels,” *Fuel processing technology*, Vol. 104, 2012, pp. 352–355.

[27] Ly, N., Majumdar, A., and Ihme, M., “Regimes of evaporation and mixing behaviors of nanodroplets at transcritical conditions,” *Fuel*, Vol. 331, 2023, p. 125870.

[28] Xiao, G., Luo, K. H., Ma, X., and Shuai, S., “A molecular dynamics study of fuel droplet evaporation in sub-and supercritical conditions,” *Proceedings of the Combustion Institute*, Vol. 37, No. 3, 2019, pp. 3219–3227.

[29] Zhang, H., and Yang, S., “Numerical investigation of high-pressure transcritical shock-droplet interaction and mixing layer using VLE-based CFD accelerated by ISAT,” *AIAA SCITECH 2023 Forum*, 2023, p. 1857.

[30] Srinivasan, N., Zhang, H., and Yang, S., “A VLE-Based Reacting Flow Solver for High-Pressure Transcritical Two-Phase Combustion,” *AIAA SCITECH 2023 Forum*, 2023, p. 1858.

[31] Zhang, H., Srinivasan, N., and Yang, S., “In Situ Adaptive Tabulation of Vapor-Liquid Equilibrium Solutions for Multi-Component High-Pressure Transcritical Flows with Phase Change,” `https://dx.doi.org/10.2139/ssrn.4534330`, 2023.

[32] Srinivasan, N., Zhang, H., and Yang, S., “Artificial Neural Network based Vapor-Liquid Equilibrium Modeling for Simulation of Transcritical Multiphase Flows,” *AIAA SCITECH Forum*, 2024.

[33] Bai, J., Lu, F., Zhang, K., et al., “ONNX: Open Neural Network Exchange,” `https://github.com/onnx/onnx`, 2019.

[34] Developers, O. R., “ONNX Runtime,” `https://onnxruntime.ai/`, 2021.

Downloaded by Suo Yang on January 4, 2024 | http://arc.aiaa.org | DOI: 10.2514/6.2024-1636